Sensors & Actuators: B. Chemical 327 (2021) 128892

Contents lists available at ScienceDirect

Sensors and Actuators: B. Chemical

journal homepage: www.elsevier.com/locate/snb

Excellent isoprene-sensing performance of In_2O_3 nanoparticles for breath analyzer applications

Qian Zheng, Jun Ho Lee, Seong-Jun Kim, Hyun-Sook Lee *, Wooyoung Lee *

Department of Materials Science and Engineering, Yonsei University, 50 Yonsei-ro, Seodaemun-gu, Seoul, 03722, Republic of Korea

ARTICLE INFO

Keywords:
Gas sensor
In_2O_3 nanoparticles
Isoprene
Breath analyzer
Miniaturized gas chromatography

ABSTRACT

We report the sensing performance of In_2O_3 nanoparticles (NPs) synthesized by a co-precipitation method for the detection of isoprene. The as-synthesized In_2O_3 NPs exhibited excellent isoprene-sensing performance compared to other previously reported isoprene sensors based on metal-oxide semiconductors. Under an exposure of 1 ppm isoprene at an optimal operating temperature of 350 ℃, the In_2O_3 NP sensor showed the highest sensing response of ~231 with a rapid response time of ~3 s. The low detection limit was approximately 0.001 ppm of isoprene. Furthermore, the In_2O_3 NP sensor showed a good long-term stability for 90 days by controlling the annealing time. In addition, for the sensor's practical applications to a breath isoprene analyzer, we tested the sensing ability of the In_2O_3 NPs by integrating the sensor into a miniaturized gas analyzer based on gas chromatography (GC). The results revealed that the In_2O_3 NP sensor is sensitive and can distinctly detect 1 ppm isoprene and 10 ppm H_2 within ~100 s in a mixture gas with other breath gases, such as acetone, CO_2, CO, and CH_4. Our study demonstrated the potential of the In_2O_3 NP sensor for application in breath isoprene analyzers by controlling the sensor's annealing time and adopting the GC system.

1. Introduction

Breath analysis technology aids in disease diagnosis and detects human metabolism by analyzing changes in the concentration of exhaled breath components. Owing to its simple and noninvasive characteristics, its application has great prospects and requires a lot of research. In 1971, Linus Pauling [1], a two-time Nobel Prize winner, discovered more than 250 characteristic substances in exhaled gas using gas chromatography (GC), which led to the rise of a new field of research in modern breath gas analysis. So far, more than 3000 volatile organic compounds (VOCs) have been found in human exhaled breath [2]. Currently, there have been reports that some VOCs in exhaled gas can be employed to diagnose certain diseases: carbon dioxide for Helicobacter pylori infection, carbon monoxide for asthma diagnosis, methane for heart transplant rejection monitoring, and hydrogen for lactose malabsorption detection [3].

Isoprene is a vital VOC formed as a byproduct during cholesterol synthesis and metabolism in the liver, and its typical breath concentration ranges from 20 to 250 ppb [4]. High blood cholesterol may be a causative factor for cardiovascular diseases, leading to millions of deaths worldwide [5]. Additionally, altered isoprene concentrations are prevalent in patients of end-stage renal disease [6], lung cancer [7], and liver disease with advanced liver fibrosis [8]. In 2013, Naim Alkhouria et al. [9], used mass spectrometry to measure the exhaled gas of 37 patients suffering from nonalcoholic fatty liver disease (NAFLD) and 23 healthy people. The results showed that the concentrations of five components, such as isoprene, acetone, trimethylamine, acetaldehyde, and pentane, contained in NAFLD exhaled breath increased, among which isoprene exhibited a significant difference.

Gas chromatography-mass spectrometry (GC-MS) and its derived methods have a high detection accuracy and can analyze unknown components in respiratory gases [10–12]. However, the sample collection and pre-processing operations of these methods are complicated and the detection time is long, which fail to meet requirements of equipment, such as portability, easy operation, and quick judgment, for point-of-care testing. Therefore, they are mostly used for laboratory breath testing. In contrast, sensors prepared using metal-oxide semiconductors (MOSs) have been widely used for VOC detection, owing to advantageous features like high sensitivity, low-cost, easy fabrication and integration, and superior safety [13]. Therefore, they can be easily incorporated into portable breath analyzers. However, until now, there are fewer reports of isoprene detection using MOS-based sensors

* Corresponding authors.
E-mail addresses: h-slee@yonsei.ac.kr (H.-S. Lee), wooyoung@yonsei.ac.kr (W. Lee).

https://doi.org/10.1016/j.snb.2020.128892
Received 8 June 2020; Received in revised form 7 August 2020; Accepted 9 September 2020
Available online 13 September 2020

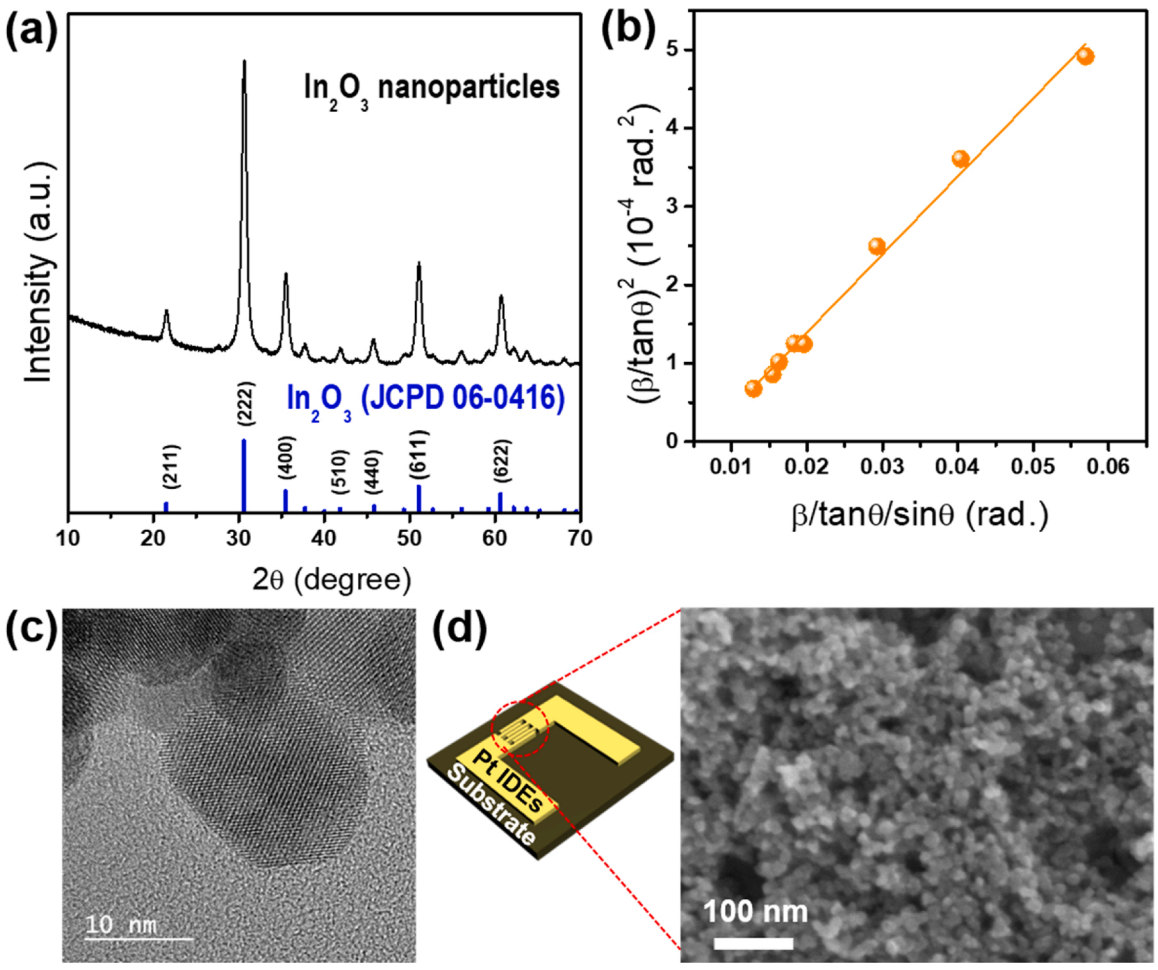

Fig. 1. (a) XRD patterns of the as-synthesized In_2O_3 NPs. The blue bars at the bottom are for the reference corresponding to cubic phase of In_2O_3 (JCPD No. 06-0416); (b) Halder-Wagner plot of In_2O_3 NPs to estimate the crystalline size; (c) TEM image of In_2O_3 NPs; (d) schematic of a sensor device and SEM image of In_2O_3 NPs dispersed on top of the interdigitated Pt electrodes after annealing.

compared to other VOC gases. In previous reports, several kinds of MOS, such as ZnO [13,14], SnO_2 [15,16], TiO_2 [17], and WO_3 [18] have been utilized for the production of isoprene-sensing materials. In contrast, indium oxide (In_2O_3) has been extensively applied to the field of VOC gas sensors [19–22] as a gas-sensing material due to its superior catalytic activity [23] and high electrical conductivity. However, reports on In_2O_3 for application in isoprene sensors are still few in number. In recent times, it has been reported that In_2O_3 is a promising potential candidate for detecting isoprene in exhaled breath [24]. To enhance sensitivity, specific surface area was significantly increased by fabricating porous flower-like microspheres of In_2O_3. The flower-like In_2O_3 microspheres exhibited commendable sensing performances at a relatively low operating temperature of 190 ℃ and could detect up to 5 ppb of isoprene. Therefore, tests on the sensing ability of In_2O_3 to detect isoprene sensitively and selectively from a gas mixture in the presence of other interfering gases are crucial for elucidating their applicability in breath isoprene analyzers.

In this paper, we investigated the isoprene-sensing performance of In_2O_3 nanoparticles (NPs) synthesized by a co-precipitation method. The as-synthesized pure In_2O_3 NPs exhibited significantly high sensing responses and a rapid response time for the detection of 1 ppm isoprene. These properties were observed in the absence of size reduction and noble metal addition, as presented in previous reports [13–24]. In particular, MOS sensors like In_2O_3 have shortcomings regarding long-term stability and selectivity that must be overcome for practical application. Here, the hindrance of long-term stability was resolved by controlling the annealing time of the In_2O_3 NP sensor. Selective detection of isoprene in a gas mixture was achieved by adopting a miniaturized GC system for further applications in portable breath analyzers.

2. Materials and methods

2.1. Synthesis of In_2O_3 nanoparticles

In_2O_3 NPs were synthesized via a co-precipitation method [25]. 1.5 g of indium nitrate hydrate ($In(NO_3)_2{\cdot}9H2O$, Sigma Aldrich, US) was dissolved in 20 ml of distilled water and stirred for 30 min at room temperature to form a homogeneous precursor. Following this, NH_4OH was added dropwise into the precursor solution until the pH of the mixed solution reached 10. Subsequently, the resultant white precipitate was rinsed thrice with ethanol using a centrifuge, and then dried at 80 ℃ for 1 d. Finally, the product was calcined at 300 ℃ for 2 h in a furnace to obtain pure In_2O_3 NPs.

2.2. Characterization

The crystalline phase of the as-synthesized In_2O_3 NPs was examined using an X-ray powder diffractometer (XRD, Ultima IV/ME 200DX, Rigaku) with a Cu-Kα radiation source. The morphology and structure of the In_2O_3 NPs were investigated by field-emission scanning electron microscopy (FE-SEM, JEOL 7001 F) and transmission electron microscopy (TEM, JEOL JEM ARM 200 F). The analysis of surface chemistry

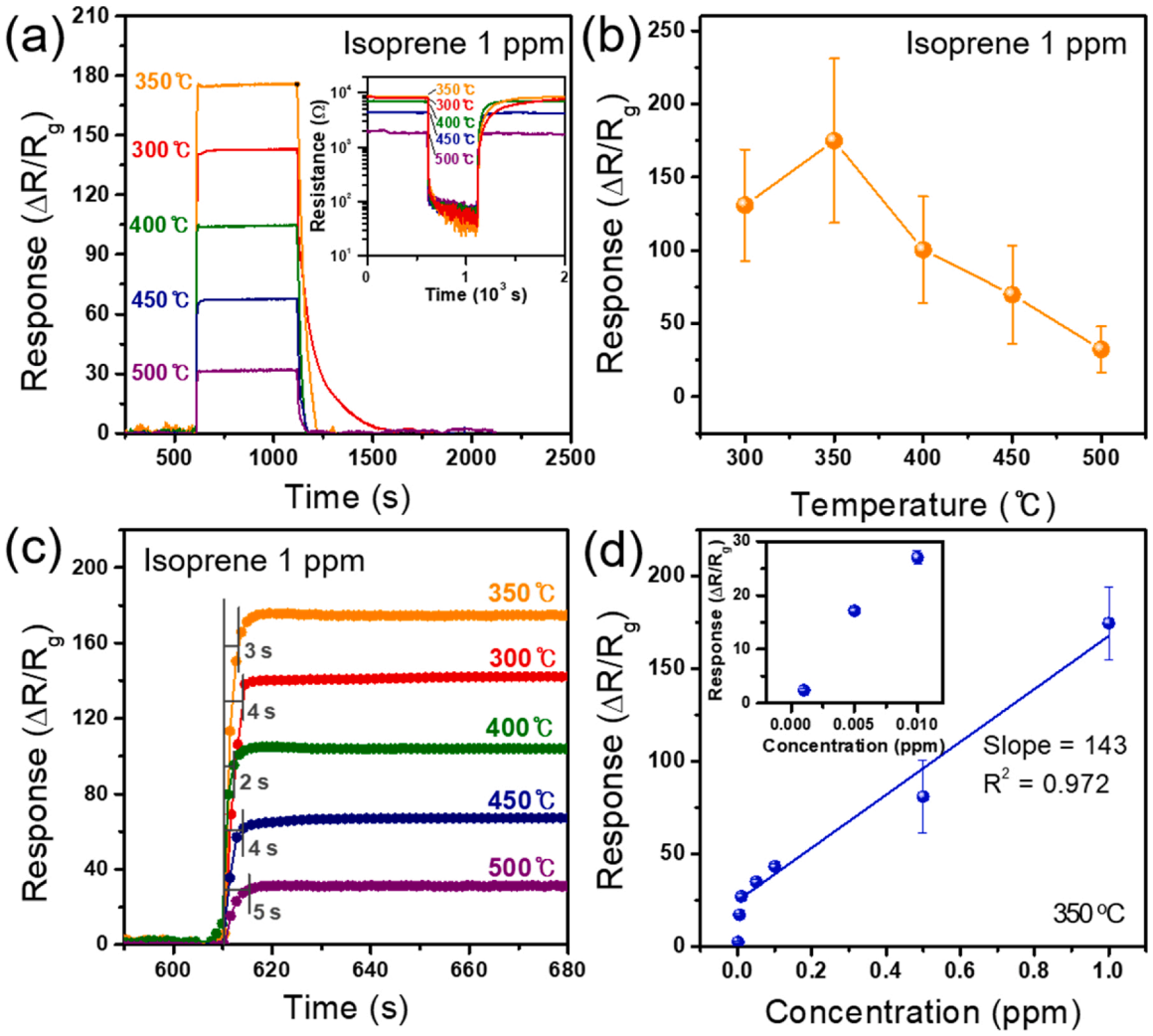

Fig. 2. (a) Variation in the response of In_2O_3 NPs to 1 ppm isoprene in the operating temperature range of 350–500 °C; (b) maximum sensing response of In_2O_3 NPs at 1 ppm isoprene as a function of operating temperature; (c) response time of In_2O_3 NPs under exposure to 1 ppm isoprene at the different operating temperatures; (d) sensing response of In_2O_3 NPs to different concentrations of isoprene in the range of 0.001 – 1 ppm at the optimal working temperatures of 350 °C. The inset shows the sensing response for the low concentration of isoprene in the range of 0.001–0.05 ppm.

was performed via X-ray photoelectron spectroscopy (XPS, K-alpha Thermo VG) with Al-Kα radiation (1486.6 eV). Additionally, the optical properties of the NPs were measured using a UV-vis spectrophotometer (UV-vis, V650 JASCO) in the wavelength range of 200–800 nm. The specific surface area of the as-prepared In_2O_3 NPs was estimated using the Brunauer-Emmett-Teller method (BET, BERLSORP-max).

2.3. Fabrication of sensor devises

Two types of sensors for sensing measurements were prepared on a SiO_2 substrate (8.5 × 8.5 mm^2) for a tube furnace system and an Al_2O_3 substrate (0.5 × 0.25 mm^2) for a miniaturized gas analyzer based on gas chromatography (mini-GC) systems. Interdigitated Pt electrodes were patterned on the substrates. The as-prepared In_2O_3 powder was dissolved in methanol to form a solution and the In_2O_3 solution was dropped on the Pt interdigitated electrode. After drying at 100 ℃, the devices were annealed at 600 ℃ for 30 min to remove the solvent and improve the mechanical and thermal stabilities of the In_2O_3 NPs.

2.4. Sensing measurements

Sensing performance of the as-synthesized In_2O_3 NPs for isoprene was tested in two types of sensing measurement systems, a tube furnace and a mini-GC system. Moreover, the tube furnace system was equipped with mass flow controllers (MFCs). The concentration of desired isoprene was adjusted using air as a balance gas by controlling the gas flow rate using the MFCs. Following this, a specific amount of isoprene gas and air was injected into the chamber at a constant flow rate of 1000 sccm. The working temperature of the In_2O_3 NPs sensor was varied using the temperature controller of tube furnace. The sensing performance of the In_2O_3 NPs was tested for various isoprene concentrations in the range 0.01–1 ppm at different operating temperatures ranging between 300 to 500 ℃. The sensing resistance was measured using a current source (Keithley 6220) and a nanovoltmeter (Keithley 2182). 10 nA of constant current was applied for a time interval of 1 s. The sensor response was defined as $\Delta R/R_g$, where $\Delta R = (R_a - R_g)$. Here, R_a and R_g are the sensor resistances in air and isoprene gas, respectively. The response time is defined as the time for the sensor to achieve 90% of the total resistance change for the target gas.

Furthermore, to elucidate the applicability of In_2O_3 NPs in breath isoprene analysis, we tested their sensing ability by integrating the sensor into the mini-GC system developed recently by our group [26]. The mini-GC system has dimensions of 6 × 8 × 13 cm^2 and consists of three main parts—a sampling loop to collect the injected gas, a packed column to separate the mixed gas, and a sensor to detect the target gas. These parts are connected by a mini pump and three solenoid valves.

The target gas mixed with the ambient carrier gas was collected into the sampling loop without pre-concentration. The total volume of the sampling loop was limited to 1 ml. The injected gas was passed through the packed column with a constant flow rate of 30 sccm. The length and inner diameter of the packed column were adjusted to 20 cm and 0.15 cm, respectively, to obtain the best sensing signal. The operating temperature of the In_2O_3 NPs sensor was varied from 300 ℃ to 500 ℃, but that of column was maintained at 25 ℃. The working temperature of the In_2O_3 NPs sensor was controlled by applying a voltage through Pt heater patterned on the backside of the Al_2O_3 substrate. In the mini-GC system, the sensor signal was obtained from the logarithmic resistance (log(R)). Thus, the sensing response the In_2O_3 NPs sensor was defined as the peak height of the sensor signal, which can be expressed as ΔSensor Signal = $(\text{Sensor Signal})_{base} - (\text{Sensor Signal})_{min}$. Here, $(\text{Sensor Signal})_{base}$ and $(\text{Sensor Signal})_{min}$ are the sensor signals of the sensor exposed to the ambient air and the target gas, respectively.

3. Results and Discussion

The characterization of the crystalline phase and morphology of the as-synthesized In_2O_3 NPs was conducted by XRD, TEM, and FE-SEM. Fig. 1(a) shows the XRD patterns of In_2O_3 NPs. The diffraction peaks are well-indexed to the crystal structure of the In_2O_3 cubic phase (JCPD No. 06-0416). Furthermore, no impurity or secondary phase was observed. The crystallite size of the In_2O_3 NPs was calculated by the Halder-Wagner method as follows:

$$\left(\frac{\beta \cdot cos\theta}{sin\theta}\right)^2 = \frac{K\lambda}{D}\frac{\beta}{tan\theta \cdot sin\theta} + 16\varepsilon^2, \quad (1)$$

where β is the integral breadth, K is the dimensionless shape factor, λ is the wavelength of the X-ray, D is the crystallite size, and ε is the average strain [27]. As can be seen in Fig. 1(b), the crystallite size can be obtained from the slope of $(\beta/\tan\theta)^2$ vs. $\beta/(\tan\theta \cdot \sin\theta)$ plot when a K value of 4/3 for the volume-weighted average size of spherical crystallites is adopted [28]. The calculated crystallite size of the In_2O_3 NPs was approximately 20.6 nm. Fig. 1(c) shows the TEM image of isolated In_2O_3 NPs. Meanwhile, Fig. 1(d) presents the SEM image of the In_2O_3 NPs dispersed on top of the interdigitated Pt electrode, displayed in the schematic of the sensor device, after annealing. It is evident from the image that the In_2O_3 NPs have a spherical shape and an average diameter of approximately 20 nm. This indicates that the particle size calculated from the XRD analysis is consistent with that obtained from the electron microscopic images. Furthermore, phase stability of the as-synthesized In_2O_3 NPs was checked after being heated under various conditions. The XRD and SEM analyses indicated that the as-synthesized In_2O_3 NPs retained its crystalline phase and morphology even after being heated at the annealing temperature of 600 °C and after sensing measurement to 1 ppm of isoprene at 350 °C (Figs. S1 and S2 in Supplementary material).

The sensing performance of the In_2O_3 NPs for 1 ppm of isoprene was first tested in the tube furnace system. Fig. 2(a) shows the variation in the sensing response over time for the In_2O_3 NPs exposed to 1 ppm isoprene at various operating temperatures ranging from 300 ℃ to 500 □. The response curves were obtained from the variations in the sensing resistance under the operating temperatures shown in the inset of Fig. 2 (a). Fig. 2(b) presents the maximum sensing response of the sensor as a function of operating temperature. The response increases with increasing operating temperature to 350 °C, and then decreases. The highest sensing response to 1 ppm isoprene was observed at 350 ℃, indicating the optimal working temperature of the In_2O_3 NP sensor. With an increase in the operating temperature, the amount of adsorbed oxygen species on the surface of the In_2O_3 NPs increases and the surface chemical reaction improves, thereby resulting in an increase in the response [29]. However, at temperatures above the optimum operating temperature, high temperatures inhibit gas adsorption, thereby reducing the response [29]. At 350 ℃, the average value of response was ~175 and the highest value was ~213. In addition, Fig. 2(c) shows that the In_2O_3 NPs have a rapid response time in the range of 2–5 s at various operating temperatures, although they have a relatively long recovery time in the range of 35–200 s (Fig. 2(a)). Response time is a crucial parameter for evaluating the sensing performance of sensors. Therefore, it can be deduced from Fig. 2(c) that when the sensor is exposed to isoprene gas, In_2O_3 NPs react immediately with the gas and reach an equilibrium state in less than 5 s. This demonstrates that the In_2O_3 NPs-based gas sensor can achieve rapid detection of isoprene gas.

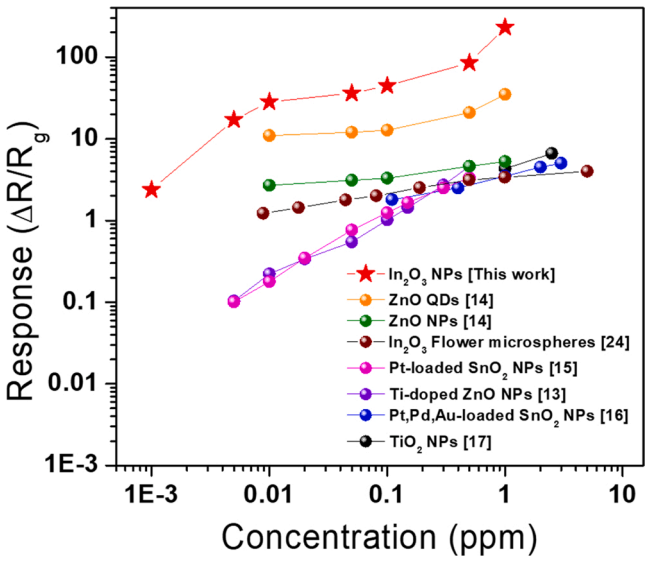

Fig. 3. Comparison of sensing response of In_2O_3 NPs to other previously reported metal-oxide semiconductor-based gas sensors for various concentration of isoprene.

Furthermore, we tested the sensing performance of the sensor for various isoprene concentrations. Fig. 2(d) shows the sensing response of the In_2O_3 NP sensor to different isoprene concentrations (0.001–1 ppm) at the optimal operating temperature of 350 ℃. It is evident that the response of the sensor increases with increasing isoprene concentration ranging from 0.01 to 1 ppm, thus demonstrating a linear relationship between the response and gas concentration (correlation coefficient, $R^2 = 0.972$). The sensitivity (slope) of the sensor in the isoprene range of 0.01–1 ppm was exceedingly high (approximately 143). Moreover, as shown in the inset of Fig. 2(d), the In_2O_3 NP sensor could detect the lowest limit of 0.001 ppm isoprene.

The sensing response of the In_2O_3 NPs exposed to various concentrations of isoprene was compared with that of the previously reported metal-oxide semiconductor-based gas sensors. As seen in Fig. 3, the In_2O_3 NPs show superior sensing response compared to the other sensors in all ranges of isoprene concentration. In addition, in terms of sensitivity, lower detection limit, and response time, the isoprene-sensing performance of the In_2O_3 NPs was significantly better than that of the other sensors, as seen in Table 1.

To understand the outstanding gas-sensing properties of the as-synthesized In_2O_3 NPs, we carried out the characterization of the surface chemistry of the In_2O_3 NPs through XPS spectral analysis. Fig. 4(a) shows the fully scanned XPS spectra of the In_2O_3 NPs, implying the existence of In and O. There are no peaks associated with other phases, such as impurities or secondary phases, which is in good agreement with the XRD results. However, a tiny C1 s peak was observed at a binding energy of ~284.6 eV. The presence of C can be explained by the generation of adventitious carbon by exposing the samples to air at room temperature during the XPS measurements [30]. Fig. 4(b) shows the high-resolution XPS spectra for In 3d. The two peaks at ~444 and ~452 eV correspond to the In $3d_{5/2}$ and In $3d_{3/2}$ spin orbits,

Table 1
Comparison of the isoprene-sensing properties of In_2O_3 NPs to various types of metal-oxide-based sensors.

Sensing materials	Operating Temperature [℃]	Concentration [ppm]	Response ($\Delta R/R_g$)	Sensitivity* [ppm^{-1}]	Detection limit [ppm]	Response time [s]	Ref.
In_2O_3 NPs	350	1	231	231	0.001	3	This work
Flower-like In_2O_3 microspheres	190	0.5	3.1	6.2	0.005	53	[24]
ZnO QDs	350	1	42	42.0	0.01	8	[14]
ZnO NPs	500	1	5.6	5.6	0.01	40	[14]
TiO_2 NPs	500	7.5	12	1.6	1	130	[17]
WO_3 NPs	350	1	4.7	4.7	0.2	20	[18]
Ti-doped ZnO NPs	325	0.5	4.6	9.2	0.005	60	[13]
Pt-doped SnO_2 NPs	400	0.5	3.3	6.6	0.005	10	[15]
(Pt,Pd,Au)-loaded SnO_2 NPs	250	2.5	5.1	2.0	0.1	60	[16]

* sensitivity = response/concentration.

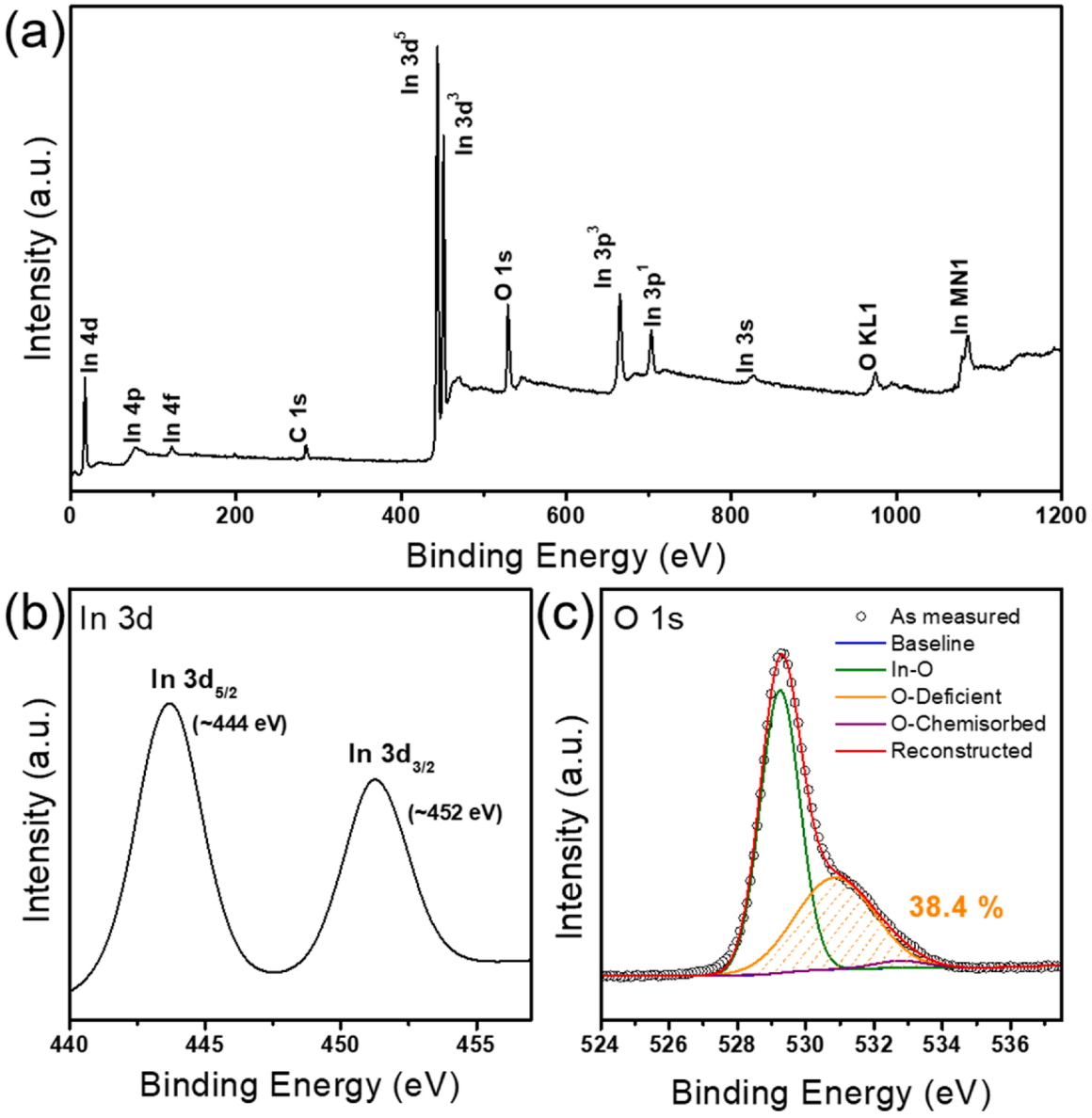

Fig. 4. (a) Wide scan XPS spectra of In_2O_3 NPs; (b) In 3d and (b) O 1s XPS spectra of In_2O_3 NPs.

respectively, representing the trivalent indium ions (In^{3+}) of In_2O_3 [31]. Fig. 4(c) shows the high-resolution XPS spectrum for O 1s state. We analyzed the oxidation state of surface elements in the In_2O_3 NPs by deconvoluting the O 1s XPS peak into three quasi-Gaussian peaks [32], as shown in Fig. 4(c). The peak centered at 529.2 eV (green line) is assigned to the lattice oxygen (O^{2-}) in the In_2O_3 phase [33], while the peak located at the higher binding energy, around 532.7 eV (purple line), corresponds to the chemisorbed oxygen species, such as H_2O and CO_2 on the surface of In_2O_3 [34]. The peak at 530.8 eV (orange line) is attributed to the oxygen vacancies in the In_2O_3 structure. Furthermore,

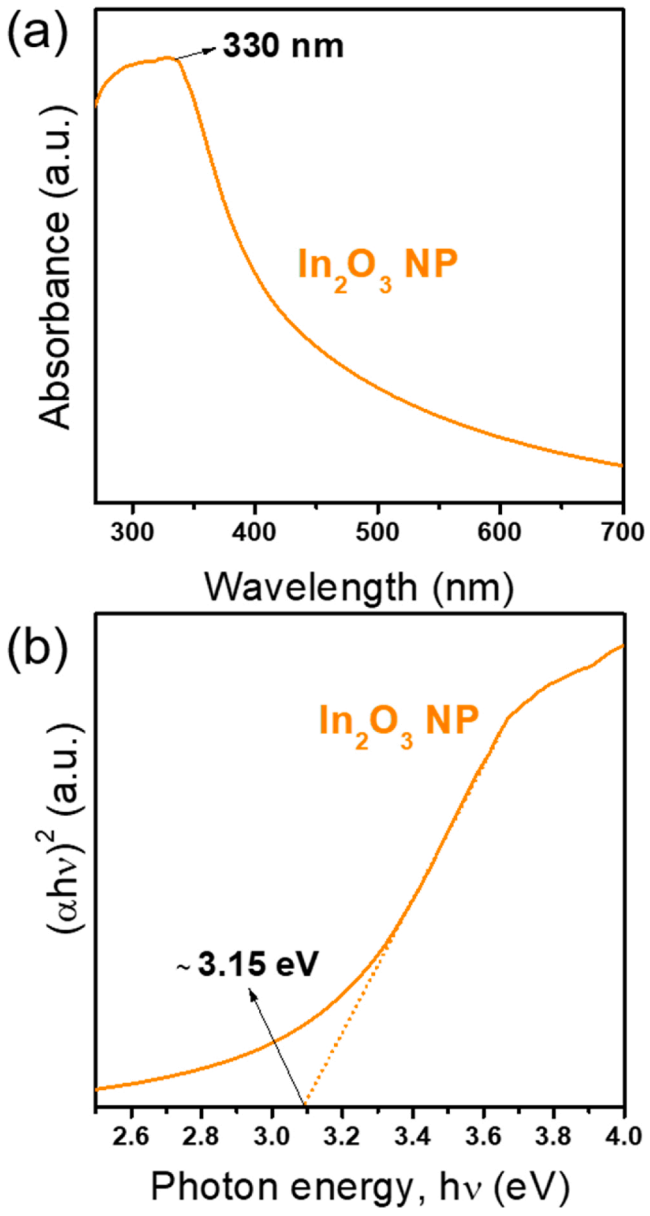

Fig. 5. (a) UV-vis absorption spectra of In_2O_3 NPs and (b) Tauc plot for optical band gap energy of In_2O_3 NPs.

the area fraction of this peak represents the oxygen-deficient ability, which is highly beneficial for enhancing the sensing performance [35,36]. Therefore, the relative percentage of the oxygen vacancies of the In_2O_3 NPs was estimated to be approximately 38.4 %.

We estimated the optical band gaps of the samples using the UV-vis absorption spectrum. As shown in the absorption spectrum in Fig. 5(a), the In_2O_3 NPs exhibited light absorption at approximately 330 nm, owing to the electronic transition from the valence band to the conduction band [37]. The optical band gap energy (E_g) was calculated using the Tauc equation for a direct band gap semiconductor as follows [38]:

$$(\alpha h\nu)^2 = A(h\nu - E_g), \quad (2)$$

where α is the absorption coefficient, h is the Planck's constant, ν is the frequency of light, and A is a constant relative to the material. The E_g value was determined from the x-intercept in the $(\alpha h\nu)^2$ versus hν plot [39], as seen in Fig. 5(b). Therefore, the estimated E_g value of the In_2O_3 NPs was 3.15 eV.

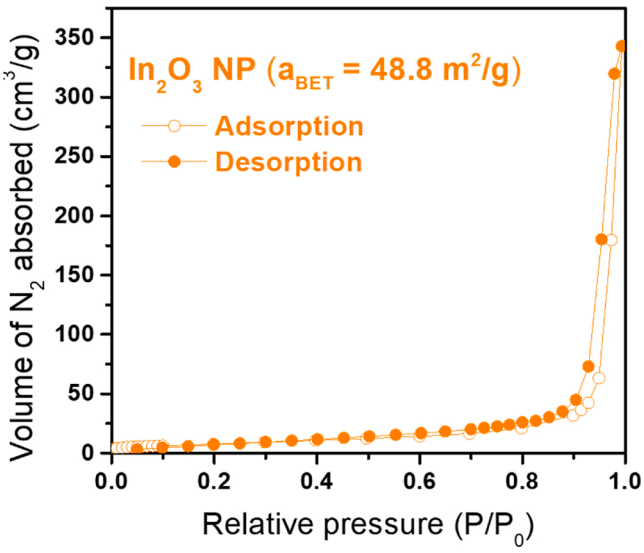

Fig. 6. N_2 adsorption-desorption isotherm of In_2O_3 NPs.

We further investigated the specific surface area of the as-synthesized In_2O_3 NPs by nitrogen adsorption-desorption method. Fig. 6 presents the N_2 adsorption-desorption isotherm of the sample. The BET specific surface area (a_{BET}) of the In_2O_3 NPs was estimated from the N_2 adsorption branches and was determined to be approximately 48.8 m^2/g.

To explain the reason for the excellent isoprene-sensing performance of the In_2O_3 NPs, the chemical and physical properties of the In_2O_3 NPs were compared with those of ZnO NPs and ZnO quantum dots (QDs) synthesized by the same wet-chemical method. The hydrothermally synthesized ZnO NPs and QDs are spherical in shape with diameters of ~25 nm and ~5 nm, respectively. The sensing response of the In_2O_3 NPs for various isoprene concentrations has already been compared with that of ZnO NPs and QDs in Fig. 3. Fig. 7 presents the sensing response to 1 ppm isoprene, oxygen vacancies, optical band gap, and specific surface areas of In_2O_3 NPs and ZnO NPs and QDs. Properties such as oxygen vacancies, optical band gap, and BET surface area, of ZnO NPs and QDs were obtained via the same methods, such as XPS, UV-vis, and BET, as described in the previous report [19]. As shown in Fig. 7(a), the In_2O_3 NPs (~20 nm) exhibited remarkably high responses even when compared to the much smaller ZnO QDs (~5 nm). Notably, the In_2O_3 NPs have a larger number of oxygen vacancies and BET specific surface areas compared to ZnO NPs and QDs, while exhibiting a lower band gap energy compared to ZnO QDs, as seen in Fig. 7(b)–(d).

It is known that smaller particles have larger specific surface areas. A larger specific surface area indicates a greater number of N_2 absorption sites on the particle surface. Therefore, the larger surface area (i.e., a great number of absorption sites) in larger particles can be attributed to the existence of larger numbers of vacant sites on the surface of the material. According to the literature, the surface oxygen vacancies are usually generated in the metal-oxide nanocluster [40,41]. It has been reported that the concentration of oxygen vacancies depends on the annealing atmosphere and temperature [42–44]. To obtain the final product, In_2O_3 NPs were annealed at 300 ℃ in air, while ZnO QDs were dried at 90 ℃. An increase in the heat treatment temperature leads to a higher concentration of oxygen vacancies [42]. Furthermore, according to theoretical calculations, the formation energy of oxygen vacancies is lower in In_2O_3 than ZnO [45]. This indicates that oxygen vacancies are more easily formed in In_2O_3 than ZnO. Consequently, a larger number of oxygen vacancies can be observed in the larger In_2O_3 NPs than in the smaller ZnO QDs, as seen in Fig. 7(b). In addition, it is known that an increase in surface oxygen vacancies would induce a larger red shift in the optical band gap (a decrease of optical band gap) [42–44].

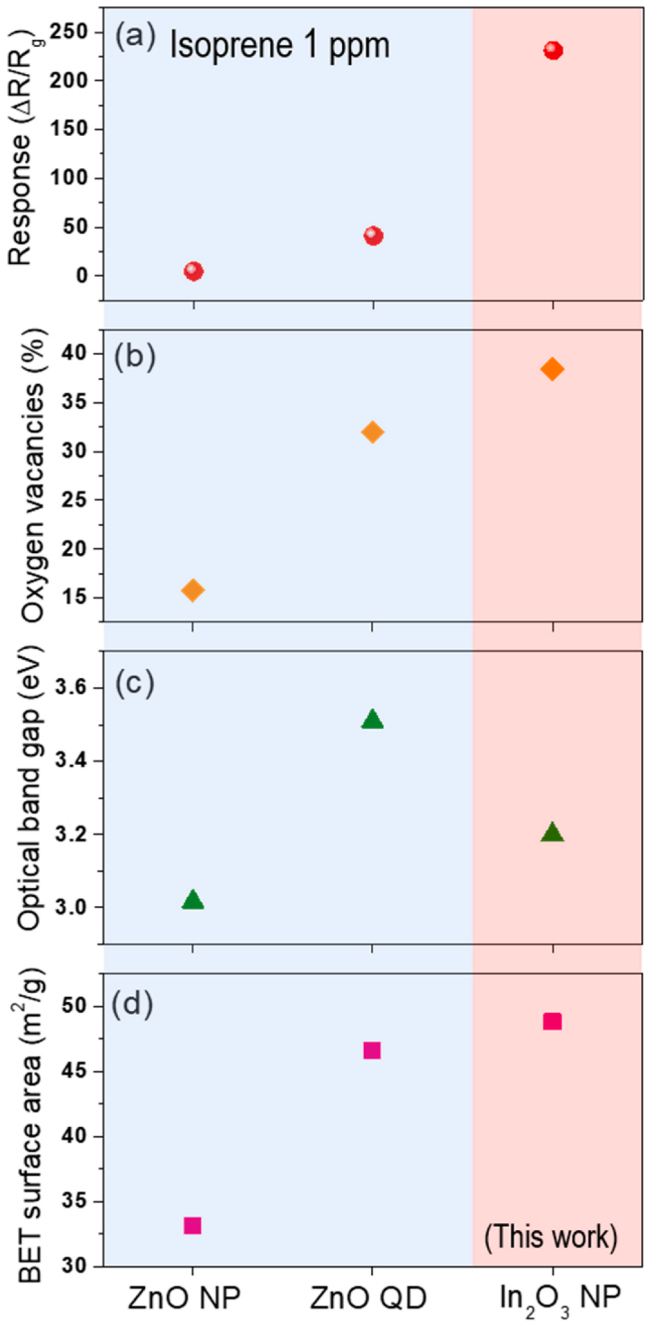

Fig. 7. Summary of the (a) sensing response, (b) oxygen vacancy, (c) optical band gap, and (d) BET surface area of In_2O_3 NPs.

Therefore, as shown in Fig. 7(c), compared to ZnO QDs, In_2O_3 NPs have a lower optical band gap. In contrast, the larger amount of oxygen vacancies is strongly associated with a greater number of reactive sites for detecting the target gas. Accordingly, the excellent sensing response of the In_2O_3 NPs compared to the ZnO NPs and QDs can be attributed to the major contribution of the increased oxygen vacancies produced in the In_2O_3 NPs.

We further investigated other sensing performance characteristics of the In_2O_3 NPs, including sensitivity to other interfering gases, reproducibility, and long-term stability at the optimal operating temperature of 350 ℃. Fig. 8(a) shows the response of the In_2O_3 NPs toward 1 ppm each of various exhaled gases, including acetone, CO, and H_2, at 350 ℃. The results showed that the In_2O_3 NPs exhibited a significantly high response for isoprene compared to the other gases. This indicates that the In_2O_3 NPs are remarkably sensitive toward isoprene. Fig. 8(b) shows the reproducibility of the In_2O_3 NPs for sensing 1 ppm of isoprene over 19 cycles at 350 ℃. The result reveals that the sensing resistance remains nearly unchanged throughout the 19 gas-in and gas-out cycles, proving the desirable repeatability characteristics of the In_2O_3 NP-based sensor for 1 ppm isoprene.

In addition, for practical applications, the humidity interference and long-term stability of the sensor was tested using different sensors prepared under various annealing times. The sensor devices were annealed at 600 ℃ for 0.5, 3, and 24 h. Fig. 8(c) shows the variation in response of the In_2O_3 NP sensors with different annealing times to 1 ppm isoprene under different humid conditions (0–90 RH%) at optimal working temperature of 350 °C. The responses of the sensors annealed with different times are ~208 for 0.5 h, ~51 for 3 h, and ~34 for 24 h at dry condition, which decrease to ~39 for 0.5 h, ~20 for 3 h, and ~13 for 24 h at 10 RH% due to a decrease in the reactive sites by adsorption of water molecules. This indicates a reduction in response of ~81%, ~61%, ~62%, respectively. However, the decreased response at 10 RH % is almost the same as that at 90 RH%.

Fig. 8(d) shows the response change of the In_2O_3 NP sensors with different annealing times under exposure to 1 ppm of isoprene at 350 ℃ and measured for 90 days. In the first measurement, the response of the sensors prepared with different annealing times is observed to be ~211 for 0.5 h, ~47 for 3 h, and ~18 for 24 h. As the annealing time increases, the sensing response decreases significantly. However, the sensor annealed for a short duration (0.5 h) exhibited significant reduction in response after 40 days. The response decreased by ~67% on the 43rd day, and after 60 days, it decreased by over 98%. However, the responses of the sensors annealed for longer durations of 3 and 24 h showed a remarkable result. The sensor responses remained nearly stable during long-time continuous measurements, as can be inferred from Fig. 8(d). After 90 days, the sensors annealed for 3 and 24 h exhibited a mean response value of 37.9 ± 5.6 and 12.9 ± 3.4, respectively.

It is noted that the response of the In_2O_3 NP sensors at 90 RH% and after 90 days is still much higher than the responses reported for other metal-oxide semiconductor-based isoprene sensors (Table 1). Therefore, the results indicate that the In_2O_3 NPs are a promising material for isoprene detection, owing to their excellent sensitivity and sensing stability. In addition, the annealing time for practical utilization of the In_2O_3 NP-based sensor should be over 3 h at 600 ℃ for optimal results.

To test the sensitive and selective detection of isoprene in human breath, which contains various VOCs, we tested the sensing ability of the In_2O_3 NPs sensor by incorporating it into a GC-based gas analyzer. Fig. 9 shows the sensing performance of the In_2O_3 NPs sensor measured by the mini-GC device manufactured by our group [26]. Fig. 9(a) shows the sensing signal as a function of time for the In_2O_3 NPs sensor integrated into the mini-GC under exposure to various concentration of N_2-balanced isoprene ($0.01 - 5$ ppm) at an operation temperature of 350 ℃. As shown in Fig. 9(a), the sensor signal curves show two peaks at ~33 s and ~94 s, implying the detection of nitrogen and isoprene gas, respectively. No obvious change of signal was detected when the isoprene concentration was lowered to 0.01 ppm. Therefore, the detection limit of the In_2O_3 NPs integrated into the mini-GC for isoprene gas sensing was estimated to be 0.05 ppm. Fig. 9(b) shows the Δ Sensor Signal for defining the peak height of the sensor signal for the various isoprene concentrations that were presented in Fig. 9(a). This represents the response of the In_2O_3 NP sensor measured via the mini-GC device. As shown in the inset of Fig. 9(b), the sensing response increases with increasing isoprene concentration ranging from 0.01 to 5 ppm. In particular, the response of the sensor has a strong linearity with isoprene ($R^2 = 0.999$) in the breath isoprene range of $0.01 - 1$ ppm, as shown in Fig. 9(b).

Further, we tested the sensing ability of the In_2O_3 NP sensor incorporated into the mini-GC device for various VOC gases found in exhaled breath at the optimal operating temperature of 350 ℃. Fig. 9(c) shows

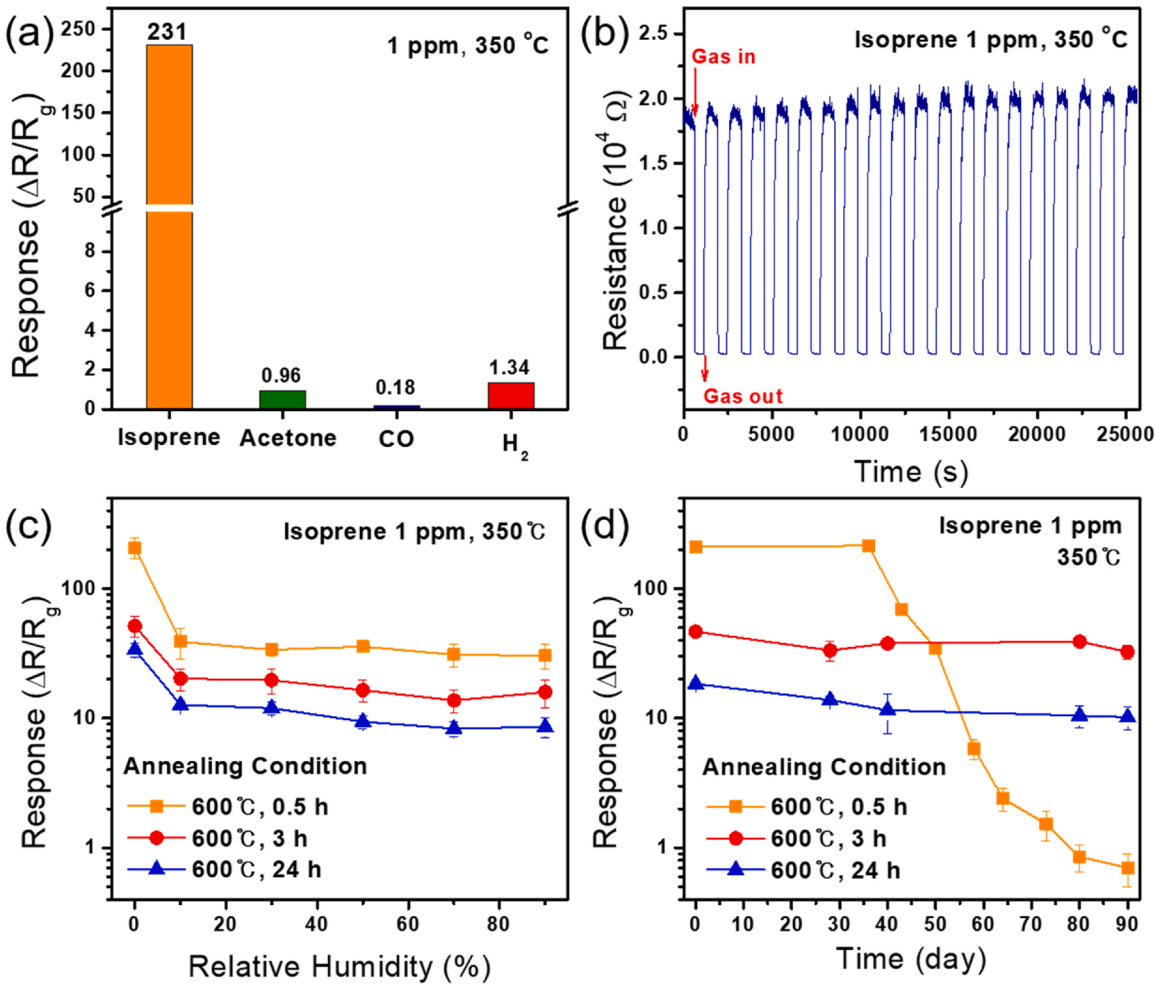

Fig. 8. (a) Sensing response of In_2O_3 NPs for 1 ppm of various gases such as acetone, CO, and H_2 at the optimal working temperature of 350 °C; (b) reliability of In_2O_3 NPs for the detection of 1 ppm isoprene over 19 cycles at 350 °C; (c) variation in the response of In_2O_3 NPs for 1 ppm isoprene as a function of relative humidity (RH) at 350 °C; (d) long-term stability of In_2O_3 NPs in sensing 1 ppm isoprene at 350 °C for 90 days.

the variations in the sensing signal of the In_2O_3 NP sensor when exposed to various target gases, such as (i) synthetic air, (ii) 1 ppm isoprene, (iii) 1 ppm acetone, (iv) 10 ppm H_2, (v) 100 ppm CO_2, (vi) 1 ppm CO, (vii) 1 ppm CH_4, and (viii) a gas mixture of all test gases. Among the aforementioned test gases, only isoprene was balanced with N_2 gas, while others were based on synthetic air. Therefore, in the case of (i)–(vii), the N_2 sensing peak is observed only when the isoprene was injected as a target gas. Particularly for 10 ppm of air-balanced H_2, only one peak was observed at ~32 s. This indicates that the In_2O_3 NP sensor incorporated into the mini-GC also can detect 10 ppm of H_2. However, there was no indication of the detection of the other gases, such as air, 1 ppm acetone, 100 ppm CO_2, 1 ppm CO, and 1 ppm CH_4, at 350 ℃.

To test the selectivity for isoprene detection, the gas mixture containing all the test gases from (ii) to (vii) was injected into the device. As shown in curve (viii) in Fig. 9(c), two peaks are observed. According to the results of (i)–(vii), the peak at 32 s is associated with N_2 and H_2, and the peak at ~100 s is solely attributed to isoprene. The result reveals that the In_2O_3 NP sensor incorporated into the mini-GC device can distinctly detect 1 ppm of isoprene from other gases within ~100 s. Consequently, we demonstrated that the In_2O_3 NPs could sensitively and selectively detect isoprene by utilizing a mini-GC, and the device exhibits potential for applicability in breath isoprene analyzers.

4. Conclusion

We investigated the isoprene-sensing properties of In_2O_3 NPs synthesized by a co-precipitation method. The In_2O_3 NP sensor demonstrated excellent sensing performance, including a high sensing response of ~231 and a fast response time of ~3 s for the detection of 1 ppm isoprene at an optimal working temperature of 350 °C. In addition, the sensor showed a good sensitivity of 143 ppm^{-1} in the isoprene concentration range of 0.01–0.1 ppm. Moreover, it can detect the lower limit of 0.001 ppm of isoprene. The isoprene-sensing performance of the In_2O_3 NP sensor was superior to the performances of previously reported metal-oxide-based sensors. According to the results of chemical and physical characterization of the material, it was found that the significantly high sensing performance of the In_2O_3 NP sensor for isoprene detection could be attributed mainly to a large number of oxygen vacancies generated during synthesis. Furthermore, we found that the sensing stability of the In_2O_3 NPs could be maintained for a long period of time (90 days) by controlling the annealing time of the sensor. More importantly, the In_2O_3 NP sensor could selectively detect 1 ppm isoprene in a mixture gas with other interfering gases, such as 10 ppm H_2, 1 ppm acetone, 100 ppm CO_2, 1 ppm CO, and 1 ppm CH_4, within ~100 s by adopting a miniaturized GC system. Accordingly, for further application of a portable breath isoprene analyzer, In_2O_3 NPs have proven to be a promising candidate sensing material. Moreover, issues of long-term stability and selectivity of the In_2O_3 NP sensor can be solved by controlling the annealing time of the sensor and adopting a mini-GC system, respectively.

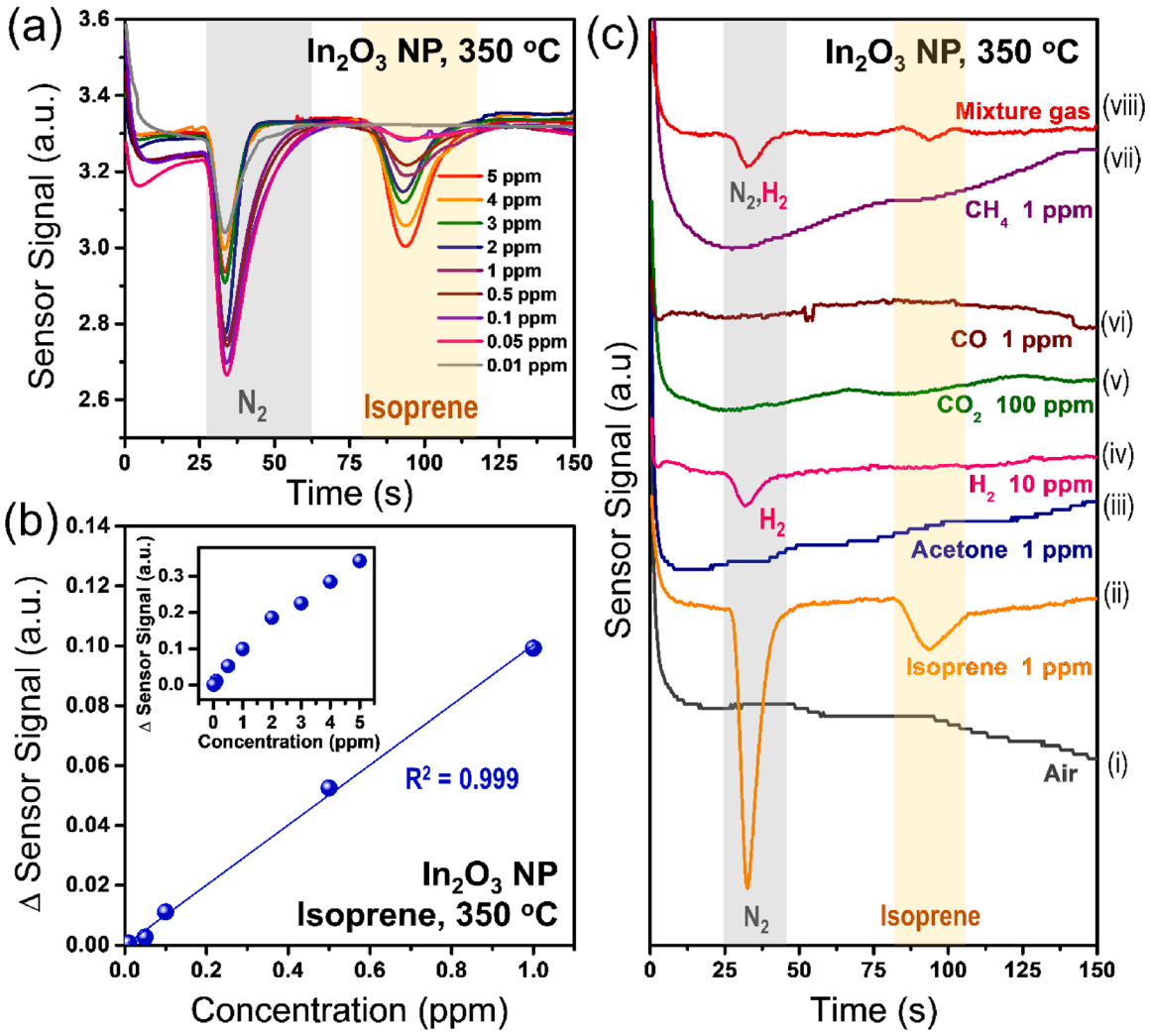

Fig. 9. Sensing performance of In_2O_3 NP sensor measured in a miniaturized gas chromatography system at the optimal operating temperature of 350 °C: (a) sensor signal changes for various isoprene concentrations (0.01 – 5 ppm); (b) peak height of the sensor signal (Δ Sensor signal) at various isoprene concentrations (0.01 – 1 ppm) (Inset: Δ Sensor signal at isoprene concentration ranging from 0.01 to 5 ppm); (c) sensor signals for (i) synthetic air, (ii) 1 ppm isoprene, (iii) 1 ppm acetone, (iv) 10 ppm H_2, (v) 100 ppm CO_2, (vi) 1 ppm CO, (vii) 1 ppm CH_4, and (viii) mixture gas of all test gases.

CRediT authorship contribution statement

Qian Zheng: Conceptualization, Investigation, Formal analysis, Validation, Writing - original draft. **Jun Ho Lee:** Investigation, Validation. **Seong-Jun Kim:** Investigation, Validation. **Hyun-Sook Lee:** Conceptualization, Validation, Writing - original draft, Writing - review & editing. **Wooyoung Lee:** Supervision.

Declaration of Competing Interest

The authors report no declarations of interest.

Acknowledgements

This research was supported by the Basic Science Research Program (2017M3A9F1052297) and the Priority Research Centers Program (2019R1A6A1A11055660) through the National Research Foundation of Korea (NRF), funded by the Ministry of Science and ICT.

Appendix A. Supplementary data

Supplementary material related to this article can be found, in the online version, at doi:https://doi.org/10.1016/j.snb.2020.128892.

References

[1] L. Pauling, A.B. Robinson, R. Teranish, P. Gray, Quantitative analysis of urine vapor and breath by gas-liquid partition chromatography, Proceedings of the National Academy of Science of the United States of America 68 (1971) 2374–2376.
[2] T.A. POPOV, Human exhaled breath analysis Ann, Allergy Asthma Immunol 106 (2010) 451–456.
[3] K.M. Paschke, A. Mashir, R.A. Dweik, Clinical applications of breath testing, F1000 Med Rep 2 (2010) 56.
[4] P. Španěl, S. Davies, D. Smith, Quantification of breath isoprene using the selected ion flow tube mass spectrometric analytical method, Rapid Commun, Mass Spectrom 13 (1999) 1733–1738.
[5] WHO, Global Health Observatory (GHO) data, 2015.
[6] S. Davies, P. Španěl, D. Smith, A new' online' method to measure increased exhaled isoprene in end-stage renal failure, Nephrol Dial Transplant 16 (2001) 836–839.
[7] A. Bajtarevic, C. Ager, M. Pienz, M. Klieber, K. Schwarz, M. Ligor, T. Ligor, W. Filipiak, H. Denz, M. Fiegl, W. Hilbe, W. Weiss, P. Lukas, H. Jamnig, M. Hackl, A. Haidenberger, B. Buszewski, W. Miekisch, J. Schubert, A. Amann, Noninvasive detection of lung cancer by analysis of exhaled breath, BMC Cancer 9 (2009) 1–16.
[8] N. Alkhouri, T. Singh, E. Alsabbagh, J. Guirguis, T. Chami, I. Hanouneh, D. Grove, R. Lopez, R. Dweik, Isoprene in the Exhaled Breath is a Novel Biomarker for Advanced Fibrosis in Patients with Chronic Liver Disease: A Pilot Study, Clin Transl Gastroenterol 6 (2015) e112.
[9] U. Alkhouri, F. Cikach, K. Eng, Analysis of breath volatile organic compounds as a noninvasive tool to diagnose nonalcoholic fatty liver disease in children, European Journal of Gastroenterology & Hepatology 26 (2014) 82–87.

[10] N. Schauer, D. Steinhauser, S. Sterelkov, GC-MS libraries for the rapid identification of metabolites in complex biological samples, FEBS Letters 579 (2005) 1332–1337.
[11] A. Ulanowska, E. Trawinska, P. Sawrycki, Chemotherapy control by breath profile with application of SPME-GC/MS method, J Sep Dci 35 (2015) 2908–2913.
[12] M. Righettoni, A. Schmid, A. Amann, Correlations between blood glucose and breath components from portable gas sensors and PTR-TOF-MS, J Breath Res 7 (2013) 37110.
[13] A.T. Güntner, N.J. Pineau, D. Chie, F. Krumeich, S.E. Pratsinis, Selective sensing of isoprene by Ti-doped ZnO for breath diagnostics, J. Mater, Chem. B Mater. Biol. Med. 4 (2016) 5358–5366.
[14] Y. Park, R. Yoo, S. Park, J.H. Lee, H. Jung, H.-S. Lee, W. Lee, Highly sensitive and selective isoprene sensing performance of ZnO quantum dots for a breath analyzer, Sens. Actuators B Chem. 290 (2019) 258–266.
[15] J. Broek, A.T. Güntner, S.E. Pratsinis, Highly Selective and Rapid Breath Isoprene Sensing Enabled by Activated Alumina Filter, ACS Sens 3 (2018) 677–683.
[16] T. Itoh, D. Lee, T. Goto, T. Akamatsu, N. Izu, W. Shin, T. Kasuga, Analysis of recovery time of Pt-, Pd-, and Au-Loaded SnO_2 sensor material with nonanal as large-molecular-Weight volatile organic compounds, Sensor Mater. 28 (2016) 1165–1178.
[17] A. Teleki, S.E. Pratsinis, K. Kalyanasundaram, P.I. Gouma, Sensing of Organic Vapors by Flame-Made TiO_2 Nanoparticles, NSTI-Nanotech 3 (2016).
[18] L. Wang, K. Kalyanasundaram, M. Stanacevic, P. Gouma, Nanosensor Device for Breath Acetone Detection, Sens. Lett. 8 (2010) 709–712.
[19] S. Elouali, L.G. Bloor, R. Binions, I.P. Parkin, C.J. Carmalt, J.A. Darr, Gas Sensing with Nano-In_2O_3 Prepared via Continuous Hydrothermal Flow Synthesis, Langmuir 28 (2012) 1879–1885.
[20] X. Sun, H. Ji, X. Li, S. Cai, C. Zheng, Mesoporous In_2O_3 with enhanced acetone gas-sensing property, Mater. Lett. 120 (2014) 287–291.
[21] P. Song, D. Han, H. Zhang, J. Li, Z. Yang, Q. Wang, Hydrothermal synthesis of porous In_2O_3 nanospheres with superior ethanol sensing properties, Sens. Actuators B Chem. 196 (2014) 434–439.
[22] S.-J. Kim, I.S. Hwang, Y.C. Kang, J.-H. Lee, Design of Selective Gas Sensors Using Additive-Loaded In_2O_3 Hollow Spheres, Sensors 11 (2011) 10603–10614.
[23] L. Liu, S. Li, X. Guo, L. Wang, L. Liu, X. Wang, The fabrication of In_2O_3 nanowire and nanotube by single nozzle electrospinning and their gas sensing property, Journal of Materials Science Materials in Electronics 27 (2016) 5153–5157.
[24] B. Han, J. Wang, W. Yang, X. Chen, H. Wang, Hydrothermal synthesis of flower-like In_2O_3 as a chemiresistive isoprene sensor for breath analysis, Sensors and Actuators B: Chemical 309 (2020), 1277788.
[25] K.W. Goh, M.R. Johan, Y.H. Wong, Enhanced structural properties of In_2O_3 nanoparticles at lower calcination temperature synthesized by co-precipitation method, Micro & Nano Letters 13 (2018) 270–275.
[26] H. Jung, W. Cho, R. Yoo, H.-S. Lee, Y.-S. Choe, J.Y. Jeon, W. Lee, Highly selective real-time detection of breath acetone by using ZnO quantum dots with a miniaturized gas chromatographic column, Sensors and Actuators B: Chemical 274 (2018) 527–532.
[27] N.C. Halder, C.N.J. Wagner, Separation of particle size and lattice strain in integral breadth measurements, Acta Cryst. 20 (1966) 312–313.
[28] T. Ida, S. Shimazaki, H. Hibino, H. Toraya, Diffraction peak profiles from spherical crystallites with lognormal size distribution, J. Appl, Crystallogr. 36 (2003) 1107–1115.
[29] X. Zhou, B. Wang, H. Sun, C. Wang, P. Sun, X. Li, X. Hu, G. Lu, Template-free synthesis of hierarchical ZnFe2O4 yolk–shell microspheres for high-sensitivity acetone sensors, Nanoscale 8 (2016) 5446–5453.
[30] Q. Xiang, G. Meng, Y. Zhang, J. Xu, P. Xu, Q. Pan, W. Yu, Ag nanoparticle embedded-ZnO nanorods synthesized via a photochemical method and its gas-sensing properties, Sens. Actuators B: Chem. 143 (2010) 635–640.
[31] S. Zhang, P. Song, H. Yan, Q. Wang, Self-assembled hierarchical Au-loaded In_2O_3 hollow microspheres with superior ethanol sensing properties, Sensors Actuat. B Chem. 231 (2016) 245–255.
[32] X.G. Han, H.Z. He, Q. Kuang, X. Zhou, X.H. Zhang, T. Xu, Z.X. Xie, L.S. Zheng, Controlling morphologies and tuning the related properties of nano/microstructured ZnO crystallites, J. Phys. Chem. C 113 (2009) 584–589.
[33] C. Chen, D. Chen, X. Jiao, S. Chen, In_2O_3 nanocrystals with a tunable size in the range of 4–10 nm: one-step synthesis, characterization, and optical properties, J. Phys. Chem. C 111 (2007) 18039–18043.
[34] B. Erdem, R.A. Hunsicker, G.W. Simmons, E.D. Sudol, V.L. Dimonie, M.S. ElAasser, XPS and FTIR surface characterization of TiO_2 particles used in polymer encapsulation, Langmuir 17 (2001) 2664–2669.
[35] J. Gan, X. Lu, J. Wu, S. Xie, T. Zhai, M. Yu, Z. Zhang, Y. Mao, S.C.I. Wang, Y. Shen, Y. Tong, Oxygen Vacancies Promoting Photoelectrochemical Performance of In_2O_3 Nanocubes, Sci. Rep. 3 (2012) 1021.
[36] H.J. Kim, H.M. Jeong, T.H. Kim, J.H. Chung, Y.C. Kang, J.H. Lee, Enhanced ethanol sensing characteristics of In_2O_3-decorated NiO hollow nanostructures via modulation of hole accumulation layers, ACS Appl. Mater. Interfaces 6 (2014) 18197–18204.
[37] G. Wang, H. Wang, Y. Ling, Y. Tang, X. Yang, R.C. Fitzmorris, C. Wang, J.Z. Zhang, Y. Li, Hydrogen-Treated TiO_2 Nanowire Arrays for Photoelectrochemical Water Splitting, Nano Lett. 11 (2011) 3026–3033.
[38] J. Tauc, Amorphous and Liquid Semiconductors, Plenum Press, New York, 1975, p. 171.
[39] R.S. Weber, Effect of local structure on the UV-Visible absorption edges of molybdenum oxide clusters and supported molybdenum oxides, J. Catal. 151 (1995) 470–474.
[40] D. Shao, L. Qin, S. Sawyer, Near ultraviolet photodetector fabricated from polyvinyl-alcohol coated In_2O_3 nanoparticles, Applied Surface Science 261 (2012) 123–127.
[41] R. Schaub, E. Wahlstrom, A. Ronnaus, E. Laegsgaard, I. Stensgaard, F. Besenbacher, Oxygen-mediated diffusion of oxygen vacancies on the TiO_2 (1 1 0) surface, Science 299 (2003) 377–379.
[42] M. Zheng, L. Zhang, X. Zhang, J. Zhang, G. Li, Fabrication and optical absorption of ordered indium oxide nanowire arrays embedded in anodic alumina membranes, Chemical Physics Letters 334 (2001) 298–302.
[43] Q. Tang, W. Zhou, W. Zhang, S. Ou, K. Jiang, W. Yu, Y.T. Qian, Size-Controllable Growth of Single Crystal $In(OH)_3$ and In_2O_3 Nanocubes, Cryst. Growth Des. 5 (2005) 147–150.
[44] G. Chen, J. Li, Synthesis of In_2O_3 nanoparticles via a green and solvent-free method, Green Process Synth 5 (2016) 389–394.
[45] I. Tanaka, F. Oba, K. Tatsumi, M. Kunisu, M. Nakano, H. Adachi, Theoretical Formation Energy of Oxygen-Vacancies in Oxides, Mater. Trans 43 (2002) 1426–1429.

Qian Zheng received a Bechelor's degree in Material Science and Engineering at Taiyuan University of Technology in 2013. Her research interests are metal oxide semiconductor-based gas sensors and their applications in breath analyzer and miniaturized GC system.

Jun Ho Lee received a Bachelor's degree and a Master's degree in Material Science and Engineering at Seoul National University in 2015 and 2017, respectively. Since 2017, he has been working on developing a miniaturized GC that is integrated with a metal oxide-based gas sensor as a researcher at Yonsei University.

Seong-Jun Kim received his Master's degree in Chemistry at Seoul National University (SNU) in 2014. He is currently completing a Ph.D. in Chemical and Biological Engineering (Y.-E. Sung group) at SNU. His research interests are focused on understanding the behavior of lithium polysulfides in Li–S batteries through synchrotron X-ray based technologies and designing new materials for energy storage. Since 2019, he has been involved in the development of gas sensors based on metal oxide semiconductors as a researcher at Nano Science and Technology Institute at Yonsei University.

Hyun-Sook Lee received a Ph.D. degree in Physics at POSTECH in 2008. Since 2015, she has been working as a research professor in the Department of Materials Science and Engineering at Yonsei University. Her research interests are in various materials related to high-temperature superconductors, solid-state hydrogen storages, rare-earth/rare-earth-free permanent magnets, and nanostructured metal oxide semiconductor gas sensors.

Wooyoung Lee is the Dean of School of Materials Science and Engineering and the Director of Institute of Nanoscience and Nanotechnology at Yonsei University in Korea. He received a BS degree in Metallurgical Engineering in 1986, a MS degree in Metallurgical Engineering from the Yonsei University in 1988. He received a Ph.D. degree in Physics from University of Cambridge, United Kingdom in 2000. He is a regular member of National Academy of Engineering of Korea. He was a member of National Science & Technology Council and a director in Korea Israel Industrial R&D Foundation. In recent years, his research interests have centered on hydrogen sensors, various metal oxide semiconducting gas sensors, and breath analyzers. He is also studying thermoelectric materials and devices, and permanent magnets. He has received a number of awards in nano-related research areas and a Service Merit Medal (2008) from the Government of Korea due to contribution on the development of intellectual properties. He has authored and co-authored over 200 publications, and has edited three special books on nano-structured materials and devices.